Article

Modeling the Polymorphism of Pentacene

Christine C. Mattheus, Gilles A. de Wijs, Robert A. de Groot, and Thomas T. M. Palstra

J. Am. Chem. Soc., **2003**, 125 (20), 6323-6330• DOI: 10.1021/ja0211499 • Publication Date (Web): 24 April 2003

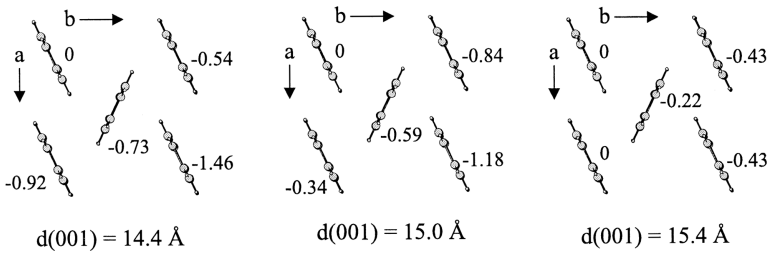

More About This Article

Additional resources and features associated with this article are available within the HTML version:

- Supporting Information
- Links to the 27 articles that cite this article, as of the time of this article download
- Access to high resolution figures
- Links to articles and content related to this article
- Copyright permission to reproduce figures and/or text from this article

View the Full Text HTML

J|A|C|S
ARTICLES
Published on Web 04/24/2003

Modeling the Polymorphism of Pentacene

Christine C. Mattheus,[†] Gilles A. de Wijs,*[,†,‡] Robert A. de Groot,[†,‡] and Thomas T. M. Palstra[†]

Contribution from the Solid State Chemistry Laboratory, Materials Science Centre, Nijenborgh 4, NL-9747 AG Groningen, The Netherlands, and Computational Materials Science, FOM Institute for Condensed Matter, Toernooiveld 1, NL-6525 ED Nijmegen, The Netherlands

Received September 5, 2002; Revised Manuscript Received March 24, 2003; E-mail: dewijs@sci.kun.nl

Abstract: Thin films of pentacene are known to crystallize in at least four different polymorphs. All polymorphs are layered structures that are characterized by their interlayer spacing *d*(001). We develop a model that rationalizes the size of the interlayer spacing in terms of intralayer shifts of the pentacene molecules along their long molecular axes. It explains the wide variety of interlayer spacings, without distorting the herringbone pattern that is characteristic of many acenes. Using two simple theoretical models, we attempt to relate the intralayer shifts with the dominant, although weak, interatomic interactions (van der Waals, weak electrostatic, and covalent). For two polymorphs, a consistent picture is found. A full understanding of the other two, substrate-induced, polymorphs probably requires consideration of interlayer interactions.

1. Introduction

Band formation in molecular organic conductors is of enormous scientific and applied interest, because it is prerequisite for achieving high values of electronic mobility. In molecular organic charge-transfer salts, band formation and high mobilities can be achieved, leading to a wealth of physical properties such as superconductivity, quantum Hall effect, etc.[1,2] Recently, it was shown that these high electronic mobilities can be observed also in single-crystal organic materials, such as C_{60},[3] utilizing space charge limited current measurements or the field effect transistor (FET) device configuration. Here, large electronic mobilities can be observed at low temperatures, resulting again in very interesting physical behavior. However, the origin of the high mobility is not well understood.

For pentacene, relatively high electronic mobilities have been reported.[4,5] Theoretical studies have reported high valence and conduction bandwidths.[6,7] Moreover, a recent combined theoretical/experimental paper reported a small reoganization energy upon positive ionization of the pentacene molecule, which also indicates that high mobilities are possible.[8] Because of the simple nature of the molecule, this material can be used as model system to study band formation. Polymorphism in pentacene is well documented.[5,9−13] Four distinctive crystalline polymorphs are known to occur and can be classified by the thickness of the molecular layers *d*(001).[5] Thus, four different structural modifications are available to study the intermolecular interactions, leading to band formation. Building on the analogy with other acenes, we propose a model that describes the microscopic structure of these polymorphs in a consistent manner. We will show that both van der Waals and electrostatic interactions are necessary to understand the stability of the particular herringbone arrangement of the molecules. We study the stability of the four different polymorphs using two complementary approaches: we model the intermolecular interactions by covalent overlap between neighboring molecules and the DREIDING force field.[14]

2. Structures of the Polymorphs

In planar aromatic hydrocarbons, two different, important intermolecular interactions can be discerned: C−H, between a carbon of the aromatic system and a hydrogen at a ring edge, and C−C, between the aromatic groups. Gavezzotti et al. have performed a database study for this class of molecular systems.[15,16] They find that all crystallize in layered structures. The intralayer structure depends on the relative abundance of C−H

[†] Solid State Chemistry Laboratory.
[‡] FOM Institute for Condensed Matter.

(1) Pope, M.; Swenberg, C. E. *Electronic Processes in Organic Crystals and Polymers*, 2nd ed.; Oxford University Press: Oxford, 1999.
(2) Ishiguro, T.; Yamaji, K. *Organic Superconductors*; Springer-Verlag: Berlin, 1990.
(3) Hebard, A. F.; Rosseinsky, R. C.; Haddon, R. C.; Murphy, D. W.; Glarum, S. H.; Palstra, T. T. M.; Ramirez, A. P.; Kortan, A. R. *Nature* **1991**, *350*, 600.
(4) Lin, Y. Y.; Gundlach, D. J.; Jackson, T. N.; Nelson, S. F.; Schlom, D. G. *IEEE Electron Device Lett.* **1997**, *18*, 87.
(5) Mattheus, C. C.; Dros, A. B.; Baas, J.; Oostergetel, G. T.; Meetsma, A.; de Boer, J. L.; Palstra, T. T. M. *Synth. Met.* **2003**, in press.
(6) Cornil, J.; Calbert, J.-P.; Brédas, J.-L. *J. Am. Chem. Soc.* **2001**, *123*, 1250.
(7) Haddon, R. C.; Chi, X.; Itkis, M. E.; Anthony, J. E.; Eaton, D. L.; Siegrist, T.; Mattheus, C. C.; Palstra, T. T. M. *J. Phys. Chem. B* **2002**, *106*, 8288.
(8) Gruhn, N. E.; da Silva Filho, D. A.; Bill, T. G.; Malagoli, M.; Coropceanu, V.; Kahn, A.; Brédas, J.-L. *J. Am. Chem. Soc.* **2002**, *124*, 7918.
(9) Dimitrakopoulos, C. D.; Brown, A. R.; Pomp, A. *J. Appl. Phys.* **1996**, *80*, 2501.
(10) Schoonveld, W. A. Ph.D. Thesis, Rijksuniversiteit Groningen, 1999.
(11) Bouchoms, I. P. M.; Schoonveld, W. A.; Vrijmoeth, J.; Klapwijk, T. M. *Appl. Phys. Lett.* **1999**, *74*, 3302.
(12) Mattheus, C. C.; Dros, A. B.; Baas, J.; Meetsma, A.; de Boer, J. L.; Palstra, T. T. M. *Acta Crystallogr., Sect. C* **2001**, *57*, 939.
(13) Brillante, A.; Della Valle, R. G.; Farina, L.; Girlando, A.; Masino, M.; Venuti, E. *Chem. Phys. Lett.* **2002**, *357*, 32.
(14) Mayo, S. L.; Olafson, B. D.; Goddard, W. A., III. *J. Phys. Chem.* **1990**, *94*, 8897.
(15) Gavezzotti, A.; Desiraju, G. R. *Acta Crystallogr., Sect. B* **1988**, *44*, 427.
(16) Desiraju, G. R.; Gavezzotti, A. *Acta Crystallogr., Sect. B* **1989**, *45*, 473.

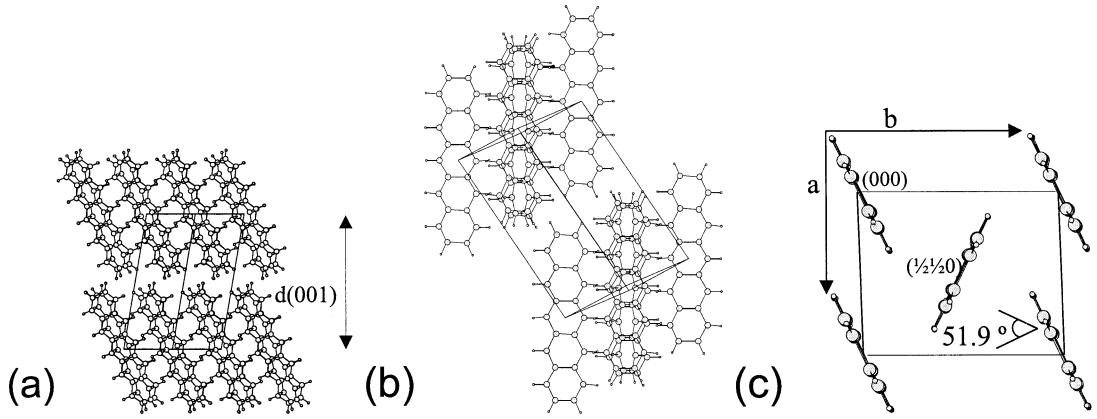

Figure 1. The crystal structure of pentacene. (a) Stacked layers of molecules in the crystal structure of pentacene, viewed along the [1$\bar{1}$0] axis. For clarity, a unit cell is also drawn. The *a* and the *b* axes are in the molecular layers, in the view of the plot they have no vertical component. (b) View approximately along **a** − **b**. Only a small shift of neighboring molecules is apparent for the direction **a** − **b**. For the direction **a** + **b** (from "upper" right to "lower" left), shifts between the molecules of approximately 1 $d_{\bigcirc}$ are apparent. (c) Projection of the pentacene crystal structure and its unit cell vectors **a** and **b** on a plane perpendicular to the long molecular axis (LMA). Viewed at this specific angle, the *a* and *b* axes seem almost orthogonal. The angle between the molecules is indicated. The herringbone arrangement is evident.

and C−C interactions. If the C−H interactions dominate, a herringbone structure is generally found. With an increasing relative number of C−C interactions, the structure becomes more graphitelike, progressing from a sandwiched herringbone, via a γ-structure, to a β-structure. In these structures, the *b* axis becomes increasingly longer, and the *a* axis becomes shorter. In the β-structure, the *a* axis is very short; it closely resembles a graphitic arrangement of the molecules.

All of the acenes, benzene through pentacene[17−19] (and several oligothiophenes[20−23] and oligophenylenes[24]), crystallize in a herringbone structure (Figure 1 depicts the herringbone structure for pentacene). This is consistent with the observations by Gavezzotti et al. as the acenes possess a relatively large number of H atoms. In view of the rather generic nature of this structure, we will try to explain the thin film polymorphs as a variation on the herringbone motif. To do so, we have to analyze the similarities and differences between the structures of all of the acenes. As the benzene molecule has a much higher symmetry than the other molecules in the series of acenes, it is omitted from the discussion.

Naphthalene,[25−27] anthracene,[19,28,29] tetracene,[30,31] and pentacene[12,31,32] have two molecules in the unit cell. The angle between the molecules (i.e., the angle between the vectors normal to the molecular planes) is remarkably similar: 52.3°, 51.1°, 51.3°, and 51.9°, respectively.

Differences are also apparent. The shorter acenes naphthalene and anthracene are monoclinic, whereas tetracene and pentacene have a lower symmetry and crystallize in a triclinic structure. In the shorter acenes, one molecule can be transformed into the other via a screw axis. In tetracene and pentacene, both molecules are crystallographically inequivalent. Only inversion symmetry is left. The inversion centers are located at the molecular centers. In the longer acenes, the long molecular axes (LMAs) have practically the same direction: for tetracene, they differ not more than 2.5°, and for pentacene, they differ not more than 1.5°. For the shorter acenes, these angles are significant: ∼22° for naphthalene and for anthracene.

The LMA in all four acenes is not oriented along the *c**-axis, but is rotated [see, e.g., Figure 1a]. For pentacene, the molecules are rotated such that they are almost parallel to the [1,1,−1] axis. This rotation is most easily characterized by relative shifts of neighboring molecules within a layer along the LMA. For the pentacene single-crystal structure, this is illustrated in Figure 2. Neighboring molecules in the direction **a** − **b** (see Figure 1b) exhibit almost no shift. However, neighboring molecules in the direction **a** + **b** are shifted considerably. These shifts are most conveniently expressed in units of one aromatic ring: $d_{\bigcirc}$ = 2.43 Å. We obtain 0.05 and 0.89 $d_{\bigcirc}$, respectively. These shifts lead to a pattern of steps within the molecular layers, as depicted in Figure 3a. The values for tetracene, 0.2 and 0.8 $d_{\bigcirc}$, respectively, are slightly different. For naphthalene and anthracene, the characterization is less exact, because the LMAs are not parallel. Nevertheless, a step pattern can be recognized. As is evident from Figure 3b, the step pattern for anthracene is qualitatively very different.

From the preceding results, we conclude that the longer acenes behave very similar. We may consider the intermolecular angle as fixed at 51.9°. The LMAs of both molecules have the same direction. Also, the lateral distances between the molecules in the molecular layers are very similar in tetracene and pentacene. Clearly, these are fixed by the C−H and C−C interactions. The only intralayer degrees of freedom left are the

(17) Cornil, J.; Beljonne, D.; Calbert, J.-P.; Brédas, J.-L. *Adv. Mater.* **2001**, *13*, 1053.
(18) Cornil, J.; Calbert, J.-P.; Beljonne, D.; Silbey, R.; Brédas, J.-L. *Adv. Mater.* **2000**, *12*, 978.
(19) Silinsh, E. A. *Organic Molecular Crystals*; Springer-Verlag: Berlin, 1980.
(20) Hotta, S.; Waragai, K. *Adv. Mater.* **1993**, *5*, 896.
(21) Horowitz, G.; Bachet, B.; Yassar, A.; Lang, P.; Demanze, F.; Fave, J. L.; Garnier, F. *Chem. Mater.* **1995**, *7*, 1337.
(22) Siegrist, T.; Fleming, R. M.; Haddon, R. C.; Laudise, R. A.; Lovinger, A. J.; Katz, H. E.; Bridenbaugh, P.; Davis, D. D. *J. Mater. Res.* **1995**, *10*, 2170.
(23) Servet, B.; Ries, S.; Trotel, M.; Alnot, P.; Horowitz, G.; Garnier, F. *Adv. Mater.* **1993**, *5*, 461.
(24) Charbonneau, G.-P.; Delugeard, Y. *Acta Crystallogr., Sect. B* **1977**, *33*, 1586.
(25) Wyckoff, R. W. G. *Crystal Structures, The Structure of Benzene Derivatives*, 2nd ed.; Interscience: New York, 1971; Vol. 6.
(26) Abrahams, S. C.; Robertson, J. M.; White, J. G. *Acta Crystallogr.* **1949**, *2*, 233.
(27) Cruickshank, D. W. J. *Acta Crystallogr.* **1957**, *10*, 504.
(28) Mason, R. *Acta Crystallogr.* **1964**, *17*, 547.
(29) Mathieson, A. M.; Robertson, J. M.; Sinclair, V. C. *Acta Crystallogr.* **1950**, *3*, 245.
(30) Campbell, R. B.; Robertson, J. M.; Trotter, J. *Acta Crystallogr.* **1962**, *15*, 289.
(31) Holmes, D.; Kumaraswamy, S.; Matzger, A. J.; Vollhardt, K. P. C. *Chem.-Eur. J.* **1999**, *5*, 3399.
(32) Siegrist, T.; Kloc, Ch.; Schön, J. H.; Batlogg, B.; Haddon, R. C.; Berg, S.; Thomas, G. A. *Angew. Chem., Int. Ed.* **2001**, *40*, 1732.

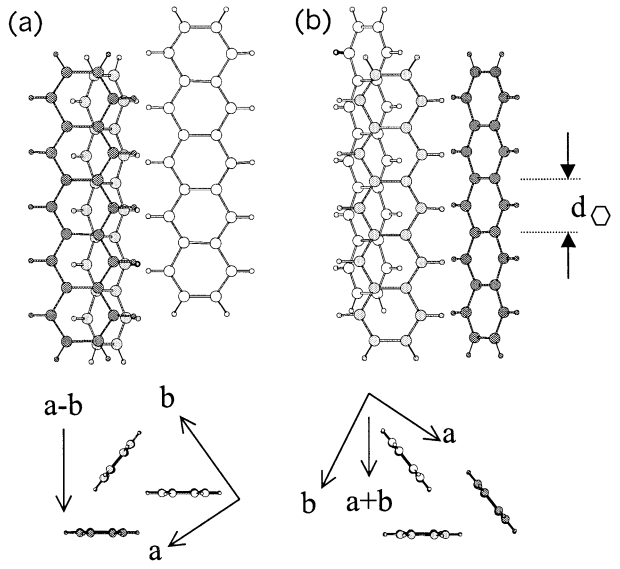

Figure 2. Projection of three pentacene molecules along various directions to show the stacking of the herringbone structure. Projection along the LMAs for neighboring molecules along (a) **a** − **b** and (b) **a** + **b** as indicated in the lower panels.

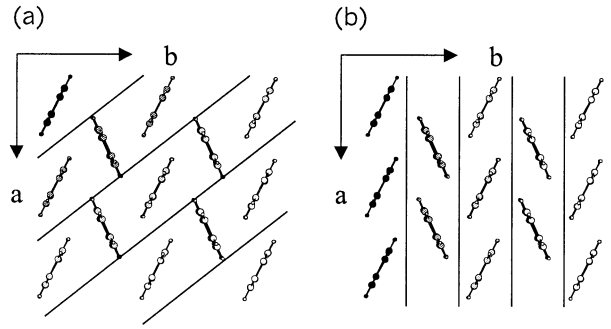

Figure 3. View along the long molecular axes of the molecules. Shifts of ∼1 $d_{\bigcirc}$ are indicated by solid lines. (a) The situation for single-crystalline pentacene, with the large shift along **a** + **b**. (b) The situation for anthracene.

relative shifts of the molecules along the LMAs. We will use these degrees of freedom to model the structure of the thin film polymorphs and thus determine *d*(001). The specific values of these shifts are fixed by experimental data on the thin film polymorphs. In section 3, we will rationalize these shifts from a careful consideration of the intermolecular interactions within the layers. First, the shift-model will be derived from the single-crystal structure, and its parameters will be defined. The model will then be used to describe the thin film polymorphs.

Figure 1c shows the result of a projection of a pentacene layer along the LMA. All distances and angles in this figure are fixed by the single-crystal data. The only parameters are the shifts of the molecules perpendicular to the plane of view. The lattice, and therefore the slant in the molecular layer, is uniquely determined by the shifts of the molecules at **a** and **b**, denoted by $\lambda_{\mathbf{a}}$ and $\lambda_{\mathbf{b}}$, respectively, relative to the molecule at (0,0,0). If inversion symmetry is present, the shift of the inequivalent molecule at ($^1/_2$,$^1/_2$,0) is $\lambda_{IE} = (\lambda_{\mathbf{a}} + \lambda_{\mathbf{b}})/2$. For the single-crystal polymorph, the LMA is close to [1,1,−1]. We approximate the shift along the LMA by a shift along [1,1,−1]. This implies that the unit cell volume is independent of $\lambda_{\mathbf{a}}$ and $\lambda_{\mathbf{b}}$ and therefore always equals the single-crystal unit cell volume. However, *d*(001) is a function of $\lambda_{\mathbf{a}}$ and $\lambda_{\mathbf{b}}$. (In section 3.2.3, we follow a slightly more sophisticated route to determine *d*(001).)

Table 1. The Reciprocal Lattice Parameters of Pentacene as Observed in Several Experiments[a]

	*a**	*b**	*c**	α*	*β**	*γ**	*d*(001)
SXD	0.1603	0.1328	0.0708	103.374	91.1114	94.91	14.12
ED1	0.1610	0.1319				89.5	
PXD	0.1563	0.1399	0.0696	102.25	92.37	98.4	14.37
ED2			0.0694				14.4
ED3	0.173	0.134				89	
ED4	0.180	0.140				89.5	
XRD1							15.0
XRD2							15.4

[a] The values of *a**, *b**, and *c** are in Å^{-1}, α*, *β**, and *γ** are in degrees, and *d*(001) values are in Å. All data are from ref 5. Each line lists an experiment, performed on different samples or different parts of a sample. SXD is single-crystal X-ray diffraction, XRD is X-ray diffraction, PXD is powder X-ray diffraction, and ED means electron diffraction.

If we take $\lambda_{\mathbf{a}} = \lambda_{\mathbf{b}} = 0$, all of the molecules stand upright at 90° angles, and the layer−layer distance (i.e., periodicity) *d*(001) ≈ 16.2 Å. [Note that 16.2 Å equals the length of the molecule (13.8 Å) plus twice the van der Waals radius of the hydrogen atom (1.2 Å).] The single-crystal structure, with *d*(001) = 14.1 Å, is obtained for $\lambda_{\mathbf{a}} = -0.84\ d_{\bigcirc}$ and $\lambda_{\mathbf{b}} = -0.94\ d_{\bigcirc}$.

As noted above, polymorphism in pentacene is well documented.[5,9−13] Four thin film polymorphs are presently known. They can be classified by the molecular layer thickness *d*(001): 14.1, 14.4, 15.0, and 15.4 Å.[12] The experimental values of the lattice parameters of the four different polymorphs are summarized in Table 1. The 14.1 and 15.0 Å polymorphs grow on Kapton, whereas the 14.4 and 15.5 Å polymorphs grow on *a*-SiO_2. As the thin film 14.1 Å polymorph has the same *d*(001), *a**, *b**, and *γ** values as the single crystal, it is assumed to be isostructural with the single crystal. For the 14.4 Å polymorph, powder X-ray diffraction (PXD) data are available. These data are sufficient to determine the cell. For the 15.0 Å (XRD1) and 15.4 Å (XRD2) polymorphs, only *d*(001) could be determined from X-ray diffraction.

Additional data on the polymorphs are available from electron diffraction (ED). The substrate is a carbon covered copper grid, that is, different from the substrates used for the X-ray diffraction measurements. Four measurements (four different spots on one sample) of *a** and *b** (or *c**) have been carried out (ED1, ED2, ED3, ED4). However (apart from ED2), direct assignment to a specific *d*(001) is not possible, as *c** could not be measured. Four different polymorphs are apparent, see Table 1. This additional data from ED can be used to characterize the thin film polymorphs. For more details, we refer to ref 5.

As two independent parameters have to be constrained, assignment of the powder X-ray data (P-XRD) and the electron diffraction experiments ED3 and ED4 is possible. $\lambda_{\mathbf{a}}$ and $\lambda_{\mathbf{b}}$ are determined by the values of *a** and *b** and listed in Table 2.

For the powder X-ray data, the shift-model accurately predicts *c** and *d*(001). The predicted angles α*, *β**, and *γ** are all off by a few degrees, although the relative sizes are well predicted. For ED3, the predicted value of *γ** is close to the experimental value; for ED4, the discrepancy is a bit larger. All deviations are acceptable. Moreover, small deviations in these angles hardly affect *d*(001). For ED3, we predict *d*(001) = 15.1 Å, and for ED4, *d*(001) = 15.9 Å. ED3 is readily assigned to the film that

Table 2. The Unit Cell Parameters (Å and Å^{-1}) of the Thin Film Polymorphs, Calculated from Their a^* and b^* Values[a]

	$\Delta\lambda_a$	$\Delta\lambda_b$	a^*	b^*	c^*	α^*	β^*	γ^*	a	b	c	α	β	γ	$d_m(001)$	$d_{AS}(001)$
SXD	0.	0.	0.1603	0.1328	0.0708	103.374	91.1114	94.91	6.266	7.775	14.53	76.475	87.682	84.684	14.12	14.12
PXD	−0.92	−0.54	0.156	0.140	0.070	108.6	88.4	93.3	6.37	7.53	15.1	71.37	90.6	87.1	14.3	14.4
ED 3	−0.34	−0.84	0.173	0.133	0.066	102.3	99.5	89.6	5.89	7.70	15.7	77.6	80.3	88.4	15.1	15.0
ED 4	0.	−0.43	0.180	0.140	0.063	107.4	105.8	84.6	5.77	7.49	17.2	73.5	75.3	91.2	15.9	15.5

[a] λ_a and λ_b are the shifts in units of d_O, that were used to construct unit cells with the specific a^* and b^* values. $d_m(001)$ is the $d(001)$ value for the shift-model. $d_{AS}(001)$ is the $d(001)$ value of the thin film polymorph to which the model structure is assigned. All $d(001)$ values are in Å.

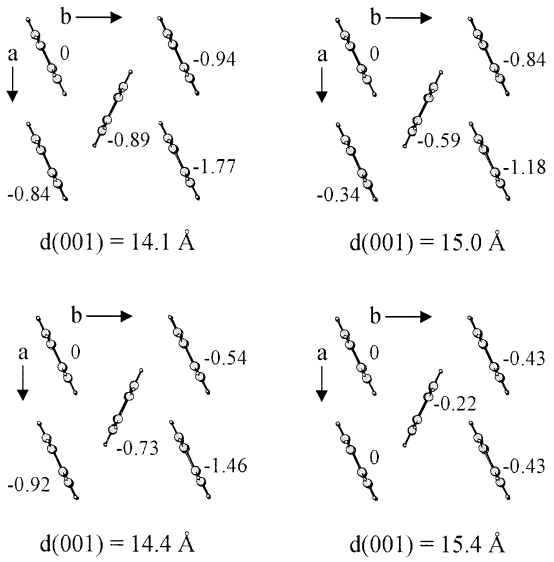

Figure 4. A schematic drawing of the crystal structures of the pentacene polymorphs. Shifts are relative to the molecule in the upper left corner.

has $d(001) = 15.0$ Å in XRD (XRD1, grown on Kapton). ED4 is assigned to the film with $d(001) = 15.4$ Å (XRD2, grown on a-SiO_2).

The assignment of all four structures is summarized in Figure 4. Inversion symmetry was assumed to determine λ_{IE}.

3. Rationalization of the Structures

Here we investigate whether it is possible to understand the proposed shifts on the basis of the intermolecular interactions. Because of their size, systems such as pentacene are outside the realm of sophisticated quantum chemical calculations. We aim to model the important interactions with as simple means as possible.

From simple geometry [e.g., Figure 1], it is evident that the most important interactions occur along $\mathbf{a} + \mathbf{b}$ and $\mathbf{a} - \mathbf{b}$. Here the hydrogens of one molecule point toward the π systems of the carbon atoms on the other, crystallographically inequivalent molecule. In the **a** direction, the hydrogen atoms of the molecules interact with other hydrogens of the periodic images.

The simplest model for the interactions is covalent overlap. It should involve filled and empty states that are sufficiently close, both in energy and spatially. In section 3.1, we use this simple model and consider the overlap of the HOMO (and HOMO−1) with the (partly empty) H states on a neighboring molecule. Covalent overlap in a molecular crystal such as pentacene will not be strong. In a second approach (section 3.2), we use a standard force field to describe the other weak interactions: the van der Waals and electrostatic forces. Thus, we have a simple, albeit approximate, description of all possibly relevant interactions. All interactions are weak and short range. Only intralayer interactions are considered. The interlayer interactions, which are direct H−H contacts, are presumably even weaker and discarded in this part of the discussion.

3.1. Overlap Model. We take the overlap between empty and filled states as a measure for the strength of the covalent interaction. The HOMO of the π system is the highest filled state. We seek empty states on the other (neighboring) molecule, that are close in energy, but also have a sizable overlap. Considering the interatomic C−H distances, the hydrogens along the $\mathbf{a} + \mathbf{b}$ or $\mathbf{a} - \mathbf{b}$ direction lie closest to the π system. Therefore, we take H functions, which are not fully filled. The H 1s state lies closest in energy to the HOMO. However, also hydrogen p orbitals are part of the LUMO and the orbitals directly above the LUMO.[33] It is difficult to exactly separate the contributions of the 1s, 2s, and 2p states to the density of states. Therefore, we take all of the hydrogen 1s, 2s, and 2p states and consider their overlap with the HOMO separately. As the HOMO−1 is only 1.1 eV below the HOMO, it is also included in the discussion.

Along the **a** direction, the adjacent molecules also lie in rather close proximity. Yet here we expect a HOMO−LUMO overlap involving the hydrogen atoms at the ends of the molecules. It should, therefore, be much weaker. Therefore, we will neglect the overlap in the **a** direction.

The overlap integral S is calculated as a function of one (or part of one) molecule relative to a neighboring molecule. We start with the overlap of one hydrogen atom (on one molecule) with the HOMO (of the other molecule) toward which it points. We then extend the model to the overlap of five hydrogen atoms (one edge of a molecule). The relative positions of the molecules are fixed to those of the single crystal. The only coordinate is the shift along the LMA relative to the neighboring molecule. Within the structural model for the polymorphs, it can be identified with $(\lambda_a + \lambda_b)/2 = \lambda_{(a+b)/2}$ or $(\lambda_a - \lambda_b)/2 = \lambda_{(a-b)/2}$. Of course, this assignment implies inversion symmetry.

3.1.1. Electron Density and Wave Functions of the Pentacene Molecule. Density functional theory (DFT) in the generalized gradient approximation (GGA, using Perdew−Wang '91)[34] was used to describe the electronic states of the molecule and to calculate the electron density of the LUMO, HOMO, and HOMO−1 (the level just below the HOMO) of pentacene. The Vienna ab initio simulation program (VASP) was employed,[35−38] using the projector augmented wave method.[39,40] The wave functions of the valence electrons electrons were expanded in plane waves. The kinetic energy cutoff was 500 eV. The molecule was placed in a periodically

(33) Mattheus, C. C. Ph.D. Thesis, Rijksuniversiteit Groningen, 2002.
(34) Perdew, J. P.; Chevary, J. A.; Vosko, S. H.; Jackson, K. A.; Pederson, M. R.; Singh, D. J.; Fiolhais, C. *Phys. Rev. B* **1992**, *46*, 6671.
(35) Kresse, G.; Hafner, J. *Phys. Rev. B* **1993**, *47*, 558.
(36) Kresse, G.; Hafner, J. *Phys. Rev. B* **1994**, *49*, 14251.
(37) Kresse, G.; Furthmüller, J. *Comput. Mater. Sci.* **1996**, *6*, 15.
(38) Kresse, G.; Furthmüller, J. *Phys. Rev. B* **1996**, *54*, 11169.
(39) Blöchl, P. E. *Phys. Rev. B* **1994**, *50*, 17953.
(40) Kresse, G.; Joubert, D. *Phys. Rev. B* **1999**, *59*, 1758.

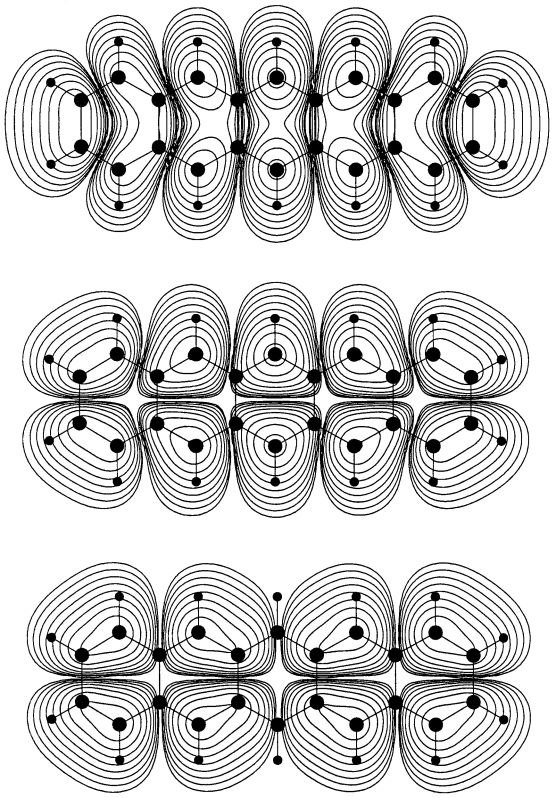

Figure 5. The calculated electron density for a pentacene molecule in a plane above the nodal plane. On top, LUMO; middle, HOMO; and bottom, HOMO−1. The large and small black circles indicate the position of the C-atoms and H-atoms, respectively. The lines are on a logarithmic scale. The lines lie at $0.0001 \times 10^{n/3}$ e/Å^3, $n \geq 1$. (n should be counted from the outermost lines. Note that the number of lines enclosing a C atom differs.)

repeated box ($20 \times 12 \times 10$ Å^3) with the LMA along the long axis of the box and the π system pointing along the short axis. The box was chosen so large that the molecule does not "feel" the presence of its periodic image; that is, effectively the charge density of a single pentacene molecule was calculated. In Figure 5, the calculated electron densities for the LUMO, HOMO, and HOMO−1 of pentacene are shown. The plane of the molecule is a nodal plane, so the electron density is shown for a plane just above the molecule. The different parts of the orbital, which are separated by nodal planes, have alternating signs. The 1s orbital of hydrogen is incorrectly calculated by DFT-GGA. Therefore, the exact wave function is used.

In many aromatic compounds, the hydrogen atoms tend to point toward the center of an aromatic ring.[41] However, in pentacene, this is not the case. As can be seen in Figure 2, the hydrogen atoms of pentacene molecules point to the side of the neighboring aromatic rings. This is consistent with the electron density of the HOMO of a pentacene molecule. The HOMO has a nodal plane along the length axis of the molecule, which makes pointing of the hydrogens to this center unfavorable.

3.1.2. Results. First, the overlap of one 1s hydrogen orbital with the HOMO was calculated. Figure 6a shows the overlap S as a function of the relative shift λ of the H atom. Zero shift corresponds to the situation where the H-orbital is pointing at the middle ring. Other maxima are observed for shifts of slightly more than 1 or 2 $d_{\bigcirc}$.

(41) Umezawa, Y.; Tsuboyama, S.; Honda, K.; Uzawa, J.; Nishio, M. *Bull. Chem. Soc. Jpn.* **1998**, *71*, 1207.

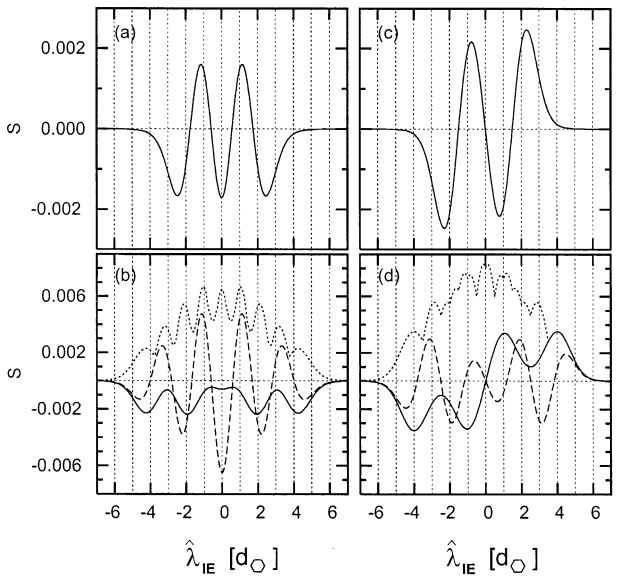

Figure 6. Top: the overlap integral (including phase factor), S, of one 1s hydrogen orbital with the HOMO (a) or HOMO−1 (c). Bottom: the overlap integral, S, for five hydrogen orbitals with the HOMO (b) and HOMO−1 (d). The dotted line was calculated without fixing the sign of the hydrogen orbitals. The hydrogens will adapt their sign to the sign of the neighboring HOMO to reach maximum overlap. The solid line was calculated with all hydrogen orbitals having the same sign. The dashed line was calculated with opposite signs for adjacent hydrogen orbitals.

The results for the overlap of five hydrogens with the HOMO can be seen in Figure 6b. The dotted line was drawn, assuming that the hydrogen orbitals do not have mutual interaction. Therefore, the phase ($\pm$) of each hydrogen orbital can adapt to the phase of the π system, and the overlap is positive for all shifts. The solid line assumes that all hydrogen orbitals of a molecule have the same sign. The dashed line is the overlap calculated, assuming that all adjacent hydrogen orbitals have alternating signs. This pattern is similar to the sign alternation of the LUMO. From the graph (dashed line), it is evident that the extrema (i.e., maximal overlap) lie at zero and almost integer multiples of $d_{\bigcirc}$. For large shifts, they shift to values a bit larger than the integer numbers. This can be understood from the electron density of the HOMO (Figure 5). Here the positions with a high electron density are shifted a little toward the ends of the molecule. Minimal overlap occurs for shifts of approximately 0.5, 1.5, 2.5, ... $\times$ $d_{\bigcirc}$. This corresponds with the nodes in the electron density of the HOMO.

Figure 6c,d depicts the overlap of the 1s H-orbital with the HOMO−1. Although the curves are different, the extrema are at approximately the same positions.

The overlap integral was also calculated for a 2s and 2p hydrogen orbital with the HOMO and HOMO−1. Because the 2s and 2p orbitals have a much larger spatial extension than the 1s orbital, the presence of two wave function extrema with opposite phase is felt. The maxima are, therefore, especially in the case of 2s, less pronounced than those for 1s. For the 2p orbital, a maximum overlap with the HOMO and HOMO−1 is reached for the same shifts as for 1s: zero and slightly more than 1 $d_{\bigcirc}$. For the 2s orbital, maxima in overlap are only reached for large shifts of 2−4 $d_{\bigcirc}$.

We now relate the calculated overlap to the proposed crystal structures of the thin film polymorphs (see Figure 4). In the case of the single crystal, the 14.1 Å structure, $\lambda_{(\mathbf{a}-\mathbf{b})/2} = (\lambda_{\mathbf{a}} -$

$\lambda_{\mathbf{b}})/2 = 0.05\ d_{\bigcirc}$ and $\lambda_{(\mathbf{a}+\mathbf{b})/2} = 0.89\ d_{\bigcirc}$. These shifts are close to 0 $d_{\bigcirc}$ and 1 $d_{\bigcirc}$ and, therefore, very near maximum overlap.

For the 14.4 Å structure, $\lambda_{(\mathbf{a}-\mathbf{b})/2} = 0.21\ d_{\bigcirc}$ and $\lambda_{(\mathbf{a}+\mathbf{b})/2} = 0.73\ d_{\bigcirc}$ were proposed. For the 15.4 Å structure, $\lambda_{(\mathbf{a}-\mathbf{b})/2} = \lambda_{(\mathbf{a}+\mathbf{b})/2} = 0.22\ d_{\bigcirc}$. The shifts for both structures are between maximum and minimum overlap.

For the 15.0 Å structure, $\lambda_{(\mathbf{a}-\mathbf{b})/2} = 0.25\ d_{\bigcirc}$ and $\lambda_{(\mathbf{a}+\mathbf{b})/2} = 0.59\ d_{\bigcirc}$. This last shift is near minimum overlap, indicating that this position is unfavorable. However, a positive or negative shift of one of the molecules by $\sim 0.5\ d_{\bigcirc}$ would place the molecules in an almost optimum configuration. It would also break the inversion symmetry of the lattice.

In the above discussion, we've only considered overlap. It's difficult to make an exact connection with binding energies. However, a rough estimate of the typical energy variations can be made using the Wolfsberg−Helmholz model. Taking an estimate of the typical variation in the overlap of 0.002, we found that the typical variation of the energy is $0.002 \times 2 \times 6.6$ eV $= 0.6$ kcal/mol/cell. Here 6.6 eV is the ionization potential,[8,42] and 2 is the number of pentacene−pentacene contacts per cell.

3.2. Model Potential Approach. In this section, we use a simple force field to model the van der Waals interactions and electrostatic interactions between the molecules. Here it is straightforward to include also the interaction between the equivalent molecules (notably the interaction between periodic images along the *a* axis). Interaction between the layers is again neglected. With the force field potential, the energies of the different pentacene polymorphs are calculated as a function of the position of the ($^1/_2$,$^1/_2$,0) molecule. So far, we assumed that inversion symmetry is preserved in all thin film polymorphs. However, when the inequivalent molecule is shifted along its length axis, the crystal structure symmetry is lowered.

3.2.1. Force Field. The DREIDING force field is used.[14] DREIDING uses general constants for the different elements, which are not dependent on the particular combinations of atoms in the structure. These constants are accurate for a large number of organic compounds.

The crystal energy is obtained as a summation over interatomic, pairwise additive interactions. The pentacene molecules themselves are kept rigid. For the van der Waals energy, a Lennard-Jones type expression is used:

$$E_{\mathrm{LJ}} = D_0[\rho^{-12} - 2\rho^{-6}] \tag{1}$$

where $\rho = R/R_0$, R (in Å) is the interatomic distance, R_0 is the van der Waals bond length, and D_0 is the van der Waals well depth. R_0 and D_0 are taken from ref 14. Electrostatic energies E_{Q} (in kcal/mol) are calculated using:

$$E_{\mathrm{Q}} = 322.0637 \times Q_i Q_j / R \tag{2}$$

where Q_i and Q_j are the charges of atoms i and j in electron units. The distribution of the charges is not known. It is used as a parameter and varied over a physically plausible range.[43,44] Calculations were carried out with $|0.1\ e|$ on the hydrogen atoms (and a compensating charge on the carbon atoms) and repeated with $|0.2\ e|$ (a recent Hartree−Fock calculation gives hydrogen charges in the range $|0.9-1.8\ e|$[45]). The leading order electrostatic interactions are between the quadrupoles of the molecules. Only interactions of molecules within a cutoff radius were included. The nearest neighbors along **a**, **b**, **a** + **b**, and **a** − **b** were taken into account, but interlayer interactions were omitted.

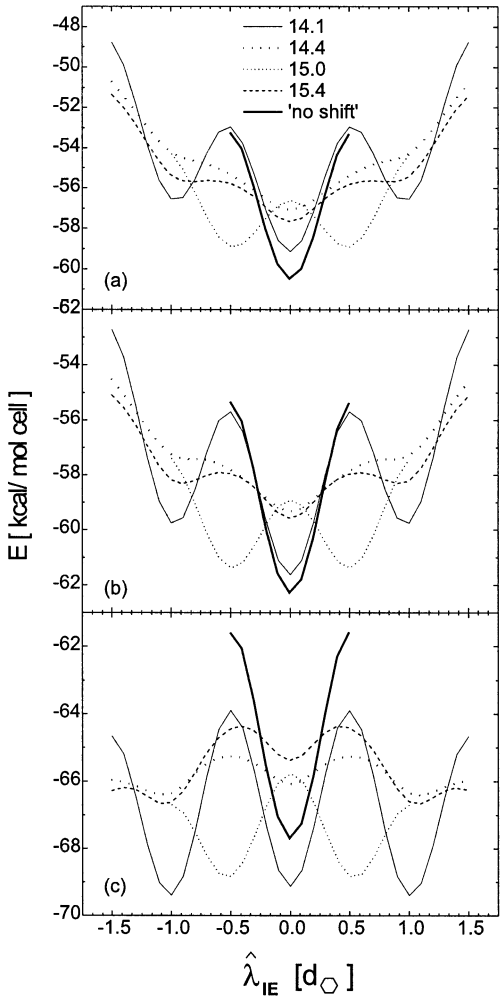

Figure 7. Energies of the different pentacene polymorphs as a function of the shift of the ($^1/_2$,$^1/_2$,0) molecule. The energy is calculated with a model potential containing only (a) a van der Waals contribution, or (b,c) both van der Waals and electrostatic contributions. The latter have a strength of (b) $|0.1\ e|$ and (c) $|0.2\ e|$.

The energy is calculated using the specific shifts, $\lambda_{\mathbf{a}}$ and $\lambda_{\mathbf{b}}$, as determined for the thin film polymorphs; that is, the cell is fixed. Only the inequivalent molecule [chosen at ($^1/_2$,$^1/_2$,0)] is allowed to shift, independently from the equivalent molecules [at (0,0,0)]. Thus, the parameter λ_{IE} is varied. The energy is plotted as a function of $\hat{\lambda}_{\mathrm{IE}} = \lambda_{\mathrm{IE}} - (\lambda_{\mathbf{a}} + \lambda_{\mathbf{b}})/2$, so that $\hat{\lambda}_{\mathrm{IE}} = 0$ corresponds to inversion symmetry of the lattice. When an energy minimum is observed, $\hat{\lambda}_{\mathrm{IE}}$ is fixed, and $\lambda_{\mathbf{a}}$ and $\lambda_{\mathbf{b}}$ are varied to check whether the minimum is stable.

3.2.2. Results. Calculations were performed for the 14.1, 14.4, 15.0, and 15.4 Å structures, and for an imaginary structure in which the molecules are not shifted. The results of the calculations with only van der Waals interactions are depicted in Figure 7a. The absolute energy minimum is attained for the structure without shifts. Minima can also be observed for the

(42) Yoon, K. B.; Kochi, J. K. *J. Phys. Chem.* **1991**, *95*, 3780.
(43) Schaftenaar, G., private communication.
(44) Williams, D. E.; Starr, T. H. *J. Comput. Chem.* **1977**, *1*, 173.
(45) Verwer, P., private communication.

14.1 and 15.0 Å structures. The 14.1 Å polymorph exhibits three minima: one around zero, and two others at 0.95 and −0.95 $d_{\bigcirc}$. The latter minima, however, lie higher in energy. This indicates that, for the 14.1 Å structure, inversion symmetry is favored above a shift of the ($^1/_2$,$^1/_2$,0) molecule. The deepest minimum of the 14.1 Å structure is only a bit higher than the minimum energy of the structure without shifts. A doubly degenerate minimum can be observed for the 15.0 Å polymorph, at shifts of 0.45 and −0.45 $d_{\bigcirc}$. A local maximum is observed for $\lambda_{IE} = 0\ d_{\bigcirc}$, so inversion symmetry is unfavorable for this structure. A shift of 0.45 $d_{\bigcirc}$, however, gives energy minima that lie almost as low as the deepest minimum of the 14.1 Å phase. This corresponds with the results of the calculated overlap integral: a shift of ∼0.5 $d_{\bigcirc}$ places the molecules in such a position that they have almost maximum overlap.

The energy curves for the 14.4 and 15.4 Å structures are similar, but clearly different from the curves for the other structures. The 14.4 and 15.4 Å structures do not have the well-defined minima that could be observed for the 14.1 and 15.0 Å polymorphs. The 14.4 and 15.4 Å structures seem to have minima at $\lambda_{IE} = 0\ d_{\bigcirc}$, $\lambda_{IE} = 0.9\ d_{\bigcirc}$, and $\lambda_{IE} = -0.9\ d_{\bigcirc}$, but these points are in fact saddle points. When varying $\lambda_{\mathbf{a}}$, we found that the energies of both the 14.4 and the 15.4 Å structures are far away from a minimum. No real minima can be observed for the 14.4 and 15.4 Å structures. Yet given the specific $\lambda_{\mathbf{a}}$ and $\lambda_{\mathbf{b}}$ for these structures, inversion symmetry is favorable.

We now add a term for Coulomb interactions to the potential, with a positive charge of 0.1 electron on the hydrogen atoms and a compensating charge on the carbon atoms.[43] The results can be seen in Figure 7b. The calculations were repeated with a charge of |0.2 *e*|. The resulting energy curves are in Figure 7c.

The additional electrostatic term does not lead to the occurrence of new minima or saddle points, but it has a marked effect on their ordering. When we only consider van der Waals interactions, the structure without shifts has the lowest lying minimum. However, if an electrostatic term (|0.1 *e*|) is switched on, this minimum shifts and becomes closer in energy to the 14.1 Å structure. With the stronger electrostatic contribution (|0.2 *e*|), it is raised to above the minima of both the 14.1 and the 15.0 Å structures. Moreover, the minima of the 14.1 and 15.0 Å structures group closely together, at a much lower energy than the 14.4 and 15.4 Å structures can attain. With increasing strength of the electrostatic contribution, the 14.1 Å structure also drops below the 15.0 Å structure and becomes the absolute minimum.

Another trend (with increasing electrostatic strength) is that the minima around 1 and −1 $d_{\bigcirc}$ of the 14.1, 14.4, and 15.4 Å structures shift downward in energy, toward the energy of the minima at $\lambda_{IE} = 0\ d_{\bigcirc}$. At |0.2 *e*|, the ordering is even reversed. This implies that the 14.1 Å structure should deform for stronger electrostatic interactions. We attribute this unphysical result to the crudeness of the model. The strength of the electrostatic potential at which the 14.1 Å polymorph becomes most stable probably is just slightly less than the strength for which it will deform and lower its symmetry.

3.2.3. Interlayer Coupling. In this section, the question of how the layers combine into a three-dimensional structure is considered in more detail. This should result in a comprehensive description of the crystal structures as well as a cleaner determination of the *d*(001) values.

Table 3. Calculated Interlayer Spacings *d*(001) for the Four (Intralayer) Model Structures[a]

structure	calculated *d*(001) (Å)
14.1 Å	14.1[A], 14.2
14.4 Å	14.3[A], 14.5
15.0 Å	15.2, 15.1
15.4 Å	15.4, 15.5

[a] Various numbers pertain to various (local) minima. Absolute minima have been labeled with an "A". The minima of the 15.0 and 15.4 Å are nearly degenerate.

The DREIDING force field as described before was employed (with a hydrogen charge |0.2 *e*|). Because the interactions within a layer are expected to be much stronger than the interactions between layers, the structure of the layers is kept fixed to the ones described in section 2.[46] The minima in energy were determined as a function of the position of one layer with respect to the adjacent layer. For all four polymorphs, an absolute and a local minimum were obtained. The results for the 14.1, 14.4, 15.0, and 15.4 Å structures are given in Table 3. A good agreement is obtained for the 14.1 Å structure: both *d*(001) and details of the single-crystal packing are reproduced; for example, interlayer contacts are predominantly mediated by hydrogens of crystallographically equivalent molecules. This is remarkable, in view of the crudeness of the model and the smallness of the interlayer interaction. The 14.4, 15.0, and 15.4 Å structures show a good agreement with the observed *d*(001) values.

4. Conclusions

On the basis of the herringbone motif, a structural model describing various pentacene thin film polymorphs and the single-crystal structure was constructed. It associates the *d*(001) values with the relative shifts of pentacene molecules within a molecular layer. The shifts could be determined for all known polymorphs (Figure 4), and the resulting values for *d*(001) were in reasonable agreement with experiments.

Two simple models were employed to rationalize the relation between the intermolecular, intralayer interactions and the polymorph's structure. The models are complementary and span the whole range of possible types of intermolecular interactions: covalent, van der Waals, and electrostatic. Both models consistently explain the 14.1 and 15.0 Å structures, provided the symmetry for the 15.0 Å polymorph is lowered to *P*1. It is well known that the electrostatic interactions play a role in stabilizing the herringbone structure for acenes.[47] We find evidence that also the rotation of the LMA away from *c** is stabilized by electrostatic interactions.

The 14.4 and 15.4 Å structures cannot be well explained with either model. The overlap model predicts them to be neither very stable nor very unstable. The force field approach shows that the internal structure of the cell is stable; that is, inversion symmetry is preserved. However, the cell itself is at a saddle point and cannot be stable.

How can we understand these discrepancies? If the 14.4 and 15.4 Å polymorphs would adopt another structure, a double

(46) To be consistent with the discussion in section 3, for the 15.0 Å structure $\lambda_{IE} = 0.5 d_{\bigcirc}$ was imposed.
(47) Williams, D. E.; Xiao, Y. *Acta Crystallogr., Sect. A* **1993**, *49*, 1.

herringbone structure would be most likely.[15,16] However, that does not fit any of the known experimental data, notably the powder diffraction on the 14.4 Å polymorph, which is perfectly consistent with a herringbone arrangement.

The most striking observation is that the 14.1 and 15.0 Å structures are grown on another substrate than are the 14.4 and 15.4 Å polymorphs (polyimide and *a*-SiO_2, respectively).[5] We therefore speculate that the specific substrate induces the growth of the 14.4 and 15.4 Å polymorphs. This points to the possible relevance of interlayer effects (note that in a study of the initial stages of pentacene growth on *a*-Si, the first molecules were lying flat on the substrate[48]). Moreover, we have argued that details in the intralayer herringbone stacking are not likely to change much. So intralayer effects seem to be ruled out.

In view of these considerations, we have to (re)consider the interlayer effects. We have assumed they are negligibly small, but we cannot rule out steric effects completely: repulsion between the H's of two layers may frustrate a shear of one layer over the other. These effects cannot be very large.[5] The strength of this interaction is sizable though, as the 14.4 Å polymorph is even stable without the support of the substrate. This suggestion is supported by Raman experiments.[49]

The reconsideration of interlayer effects also motivated the calculation of the interlayer distance with the DREIDING force field. There is a qualitative similarity between the calculated layer stackings (local minima) found for the 14.1 and 14.4 Å polymorphs (a similarity is also observed for the other pair of polymorphs). The 14.1 Å structure is known from X-ray diffraction: interlayer interactions are predominantly mediated by hydrogens on crystallographically equivalent molecules. A similar layer stacking is observed for one of the model layer structures. It is this stacking that we assign to the 14.1 Å polymorph. Raman experiments suggest that for the 14.4 Å (and 15.4 Å) polymorph, also interactions between crystallographically different molecules occur.[49] Consistently, the model calculations predict also another layer stacking (local minimum), which we assign to the 14.4 Å polymorph.

Recently, Brillante et al.,[13] using Raman spectroscopy, have provided evidence that, apart from the well-known single-crystal structure,[12,31,32] another single-crystalline polymorph exists. Following Venuti et al.,[50] it was proposed to correspond to the structure originally reported by Campbell et al.[30] As the Campbell structure has $d(001) \approx 14.5$ Å, this structure is another candidate for the thin film 14.5 Å polymorph. However, the powder X-ray diffraction results for the thin film 14.4 Å polymorph are inconsistent with Campbell's structure.[5] Presently, insufficient data are available for this new single-crystalline polymorph to attempt a description with our model.

In conclusion, a comprehensive model description of pentacene polymorphs was presented. Intralayer relative shifts of the molecules are sufficient to give a reasonable picture of the structure, including its $d(001)$. The structures can only be partially rationalized on the basis of intralayer interactions, and an extension to interlayer interactions seems desirable.

Acknowledgment. We acknowledge fruitful interactions with Dr. G. Schaftenaar, Dr. P. Verwer, Dr. A. Meetsma, and Prof. E. Vlieg. This work is part of the research program of the "Stichting voor Fundamenteel Onderzoek der Materie (FOM)", which is financially supported by the "Nederlandse Organisatie voor Wetenschappelijk Onderzoek (NWO)".

JA0211499

(48) Meyer zu Heringdorf, F. J.; Reuter, M. C.; Tromp, R. M. *Nature* **2001**, *412*, 517.
(49) Mattheus, C. C.; van Bentum, P. J. M.; de Groot, R. A.; Palstra, T. T. M.; de Wijs, G. A., in preparation.
(50) Venuti, E.; Della Valle, R. G.; Brillante, A.; Masino, M.; Girlando, A. *J. Am. Chem. Soc.* **2002**, *124*, 2128.